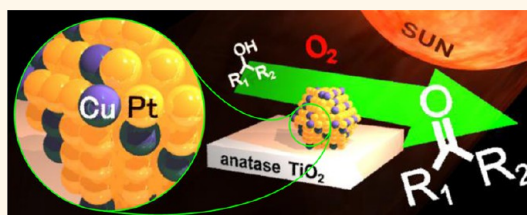


# Pt–Cu Bimetallic Alloy Nanoparticles Supported on Anatase TiO<sub>2</sub>: Highly Active Catalysts for Aerobic Oxidation Driven by Visible Light

Yasuhiro Shiraishi,<sup>†,\*</sup> Hirokatsu Sakamoto,<sup>†</sup> Yoshitsune Sugano,<sup>†</sup> Satoshi Ichikawa,<sup>‡</sup> and Takayuki Hirai<sup>†</sup>

<sup>†</sup>Research Center for Solar Energy Chemistry and Division of Chemical Engineering, Graduate School of Engineering Science, and <sup>‡</sup>Institute for NanoScience Design, Osaka University, Toyonaka 560-8531, Japan

**ABSTRACT** Visible light irradiation ( $\lambda > 450$  nm) of Pt–Cu bimetallic alloy nanoparticles (~3–5 nm) supported on anatase TiO<sub>2</sub> efficiently promotes aerobic oxidation. This is facilitated *via* the interband excitation of Pt atoms by visible light followed by the transfer of activated electrons to the anatase conduction band. The positive charges formed on the nanoparticles oxidize substrates, and the conduction band electrons reduce molecular oxygen, promoting photocatalytic cycles. The apparent quantum yield for the reaction on the Pt–Cu alloy catalyst is ~17% under irradiation of 550 nm monochromatic light, which is much higher than that obtained on the monometallic Pt catalyst (~7%). Cu alloying with Pt decreases the work function of nanoparticles and decreases the height of the Schottky barrier created at the nanoparticle/anatase heterojunction. This promotes efficient electron transfer from the photoactivated nanoparticles to anatase, resulting in enhanced photocatalytic activity. The Pt–Cu alloy catalyst is successfully activated by sunlight and enables efficient and selective aerobic oxidation of alcohols at ambient temperature.



**KEYWORDS:** photocatalysis · visible light · nanoparticles · alloy · titanium dioxide

Aerobic oxidation by heterogeneous catalysts with molecular oxygen (O<sub>2</sub>) is an indispensable process for the synthesis of chemicals from the viewpoint of green chemistry.<sup>1</sup> Photocatalytic oxidation with O<sub>2</sub> has also been studied extensively with semiconductor titanium dioxide (TiO<sub>2</sub>);<sup>2–6</sup> several types of substrates such as alcohols, amines, hydrocarbons, and sulfides are successfully oxidized at atmospheric pressure and room temperature. One of the critical issues for practical application of the photocatalytic processes is the low catalytic activity under irradiation of visible light ( $\lambda > 400$  nm), the main component of solar irradiance. Several TiO<sub>2</sub> materials doped with nitrogen,<sup>7,8</sup> sulfur,<sup>9,10</sup> carbon,<sup>11,12</sup> or boron atoms<sup>13,14</sup> have been proposed to extend the absorption edge into the visible region. These doped catalysts, however, suffer from low quantum yields for reaction (<0.5%) because they inherently contain a large number of crystalline lattices that behave as charge recombination centers.<sup>15</sup> Design of visible-light-driven

catalysts that promote efficient aerobic oxidation is still a challenge.

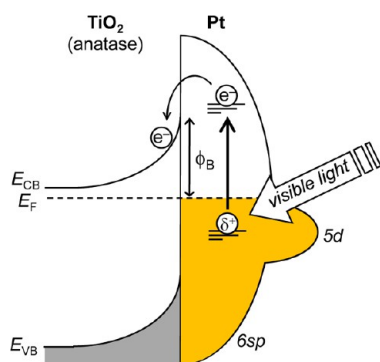
Metal nanoparticle/semiconductor heterojunction is one powerful system for the creation of photocatalysts activated by visible light.<sup>16</sup> Earlier, we reported that gold (Au) nanoparticles loaded on TiO<sub>2</sub> promote aerobic oxidation under visible light.<sup>17</sup> The reaction is promoted *via* the absorption of visible light by the Au nanoparticles due to the resonant oscillation of free electrons coupled by light, known as localized surface plasmon resonance.<sup>16</sup> Collective oscillation of 6sp band electrons (e<sup>-</sup>) on the surface Au atoms promotes *intra*band transition to the sp conduction band. The e<sup>-</sup> is transferred to the TiO<sub>2</sub> conduction band. The positive charge formed on the surface of Au particles oxidizes the substrate, while the e<sup>-</sup> on the TiO<sub>2</sub> conduction band is consumed by the reduction of O<sub>2</sub>. This catalytic cycle successfully promotes aerobic oxidation of substrates even at room temperature. The apparent quantum yield for oxidation of alcohol determined by the irradiation of

\* Address correspondence to shiraish@cheng.es.osaka-u.ac.jp.

Received for review July 30, 2013 and accepted September 24, 2013.

Published online September 24, 2013  
10.1021/nn403954p

© 2013 American Chemical Society



**Scheme 1.** Proposed mechanism for electron transfer from photoactivated Pt particles to anatase.  $E_F$  and  $\phi_B$  denote the Fermi level and the height of the Schottky barrier, respectively.

550 nm monochromatic light is 3.8%, which is much higher than that obtained with the doped catalysts (<0.5%).<sup>7–14</sup> The metal/semiconductor system is chemically stable even under aerated conditions as compared to the doped catalysts and shows a potential as a visible-light-driven catalyst.

Platinum (Pt) nanoparticles also absorb light in the visible region due to the *interband* transition of 5d band  $e^-$  to the sp conduction band,<sup>18</sup> as schematically shown in Scheme 1. Very recently, we found that Pt nanoparticles loaded on anatase  $\text{TiO}_2$  (Pt/anatase) efficiently promote aerobic oxidation under visible light irradiation.<sup>19</sup> The apparent quantum yield for the reaction is 7.1% (550 nm), which is much higher than that obtained with the Au catalyst (3.8%). The very high activity is due to the strong affinity between Pt nanoparticles and the anatase surface.<sup>20</sup> This facilitates efficient  $e^-$  transfer from the photoactivated Pt particles to anatase.

We then explored further activity improvement of the Pt/anatase system. The rate-determining step for this system is the  $e^-$  transfer from photoactivated nanoparticles to anatase. As shown in Scheme 1, the metal/semiconductor heterojunction creates a Schottky barrier ( $\phi_B$ ) at the interface.<sup>21</sup> Photoactivated  $e^-$  on the Pt particles must therefore overcome this barrier and is transferred to anatase. This implies that the height of  $\phi_B$  strongly affects the efficiency for  $e^-$  transfer. The  $\phi_B$  is defined as the difference between the work function of metal ( $W$ ) and the electron affinity of the semiconductor conduction band ( $\chi$ ):<sup>22</sup>

$$\phi_B = W - \chi \quad (1)$$

It is well-known that the work function of metal decreases by the alloying of other metal components with a lower work function.<sup>23,24</sup> This suggests that alloying of other metal with Pt would decrease the work function of Pt nanoparticles. This may decrease  $\phi_B$  and promote efficient  $e^-$  transfer from nanoparticles to anatase.

Here we report that bimetallic alloy nanoparticles consisting of Pt and copper (Cu), supported on anatase  $\text{TiO}_2$ , significantly enhance aerobic oxidation under visible light. The apparent quantum yield for the reaction, 17% (550 nm), is more than double that obtained with monometallic Pt catalyst (7.1%).<sup>19</sup> The activity of this alloy system depends strongly on the mole ratio of Pt and Cu and the size of alloy particles. The catalyst loaded with alloy nanoparticles, consisting of 80 mol % of Pt and 20 mol % of Cu with 3–5 nm diameter, exhibits the highest activity. The catalyst is successfully activated by sunlight and enables efficient and selective aerobic oxidation of alcohols at ambient temperature.

## RESULTS AND DISCUSSION

**Preparation and Properties of Bimetallic Catalysts.** Pt–Cu bimetallic alloy particles were loaded on anatase  $\text{TiO}_2$  (Japan Reference Catalyst, JRC-TIO-1; average particle size, 21.1 nm; Brunauer–Emmett–Teller (BET) surface area,  $81 \text{ m}^2 \text{ g}^{-1}$ ) by the impregnation of Pt and Cu precursors followed by reduction with  $\text{H}_2$ .<sup>25,26</sup> Anatase particles were added to water containing  $\text{H}_2\text{PtCl}_6$  and  $\text{Cu}(\text{NO}_3)_2$ , and the water was evaporated with stirring. The resultant mixture was calcined in air for 2 h and reduced with  $\text{H}_2$  for 2 h at 673 K, affording  $\text{Pt}_{1-x}\text{Cu}_x/\text{anatase}$  catalysts as brown powders. The total metal loading on the support is set at 0.4 mol % [= (Pt + Cu)/anatase  $\times$  100], and  $x$  denotes the mole fraction of Cu in the alloy [ $x = \text{Cu}/(\text{Pt} + \text{Cu})$ ].

Figure 1a shows a typical transmission electron microscopy (TEM) image of  $\text{Pt}_{0.8}\text{Cu}_{0.2}/\text{anatase}$ . Small nanoparticles were highly dispersed on the support. As shown in Figure 1c–h, high-resolution TEM images showed metal particles indexed as face-centered cubic (fcc) cuboctahedron structures. The average diameter of the particles ( $d$ ) was calculated to be 3.4 nm (Figure 1b). As shown in Figure S1 (Supporting Information),  $\text{Pt}_1/\text{anatase}$ ,  $\text{Pt}_{0.4}\text{Cu}_{0.6}/\text{anatase}$ , and  $\text{Cu}_1/\text{anatase}$  catalysts contain metal particles with similar diameters (3.3, 3.4, and 3.3 nm, respectively), indicating that Cu alloying scarcely affects the size of metal particles.

X-ray photoelectron spectroscopy (XPS) of the alloy catalysts (Figure S2, Supporting Information) shows Pt 4f peaks (70 and 74 eV) and a Cu 2p peak ( $\sim 932$  eV).<sup>27</sup> As observed for related Pt–Cu alloy systems,<sup>28–30</sup> the increase in Cu amount shifts the Cu peak to lower binding energy due to the expansion of atomic distance, although the Pt peak scarcely shifts. The surface Pt/Cu ratio of metal particles on  $\text{Pt}_{0.8}\text{Cu}_{0.2}/\text{anatase}$  determined by XPS analysis is 4.02 mol/mol. This is similar to the ratio of the total amount of Pt and Cu (3.95 mol/mol) in the catalysts determined by the inductively coupled plasma (ICP) analysis and the average Pt/Cu ratio (3.90 mol/mol) determined by the energy-dispersive X-ray spectroscopy (EDX) of some metal particles (Figure S3, Supporting Information).

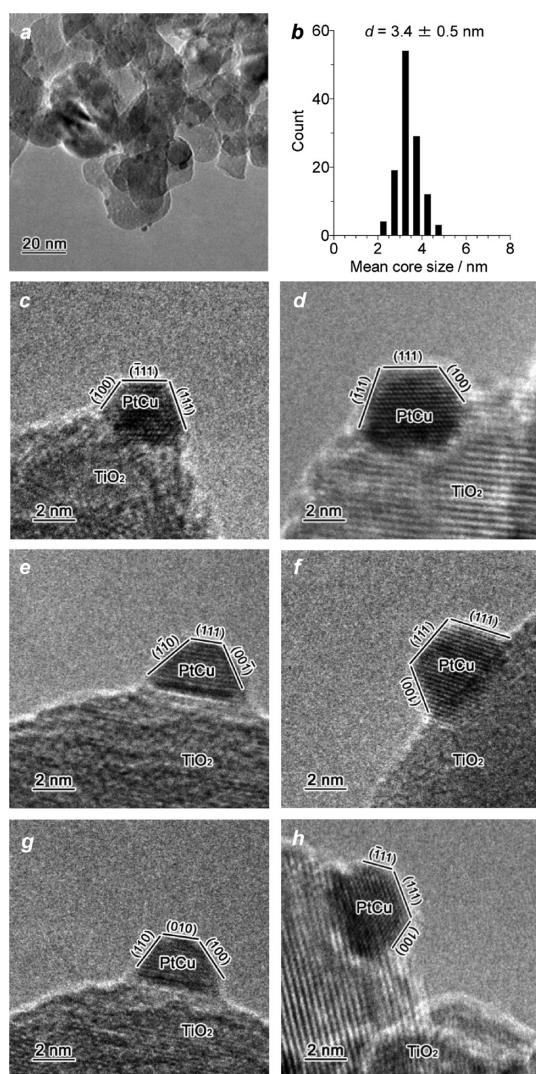


**Figure 1.** (a) Typical TEM image of  $\text{Pt}_{0.8}\text{Cu}_{0.2}$ /anatase catalyst (0.4 mol % of metal loading) and (b) size distribution of metal particles. (c–h) High-resolution TEM images.

In addition, as shown in Figure 1c–h, the lattice spacing of alloy particles (111) determined by TEM observation (0.223 nm) is between the lattice spacing for standard Pt(111) (JCPDS 04-0802, 0.226 nm) and Cu(111) (JCPDS 04-0836, 0.209 nm) and is the same as the value calculated based on Vegard's law (0.223 nm). These data suggest that Pt and Cu components in the alloy particles are mixed homogeneously. As shown in Figure 2, diffuse-reflectance UV–vis spectrum of  $\text{Pt}_1$ /anatase shows a broad absorption band at  $\lambda > 400$  nm, assigned to the interband transition of Pt particles.<sup>31</sup>  $\text{Cu}_1$ /anatase shows similar absorption at  $\lambda > 400$  nm, assigned to the light scattering by the Cu particles.<sup>32,33</sup> As a result of this, Pt–Cu alloy catalysts exhibit similar absorption spectra independent of their Pt/Cu ratio.

**Photocatalytic Activity of Alloy Catalysts.** The activity of alloy catalysts was tested by oxidation of benzyl alcohol, a typical aerobic oxidation.<sup>34</sup> The reactions were performed by stirring a toluene solution (5 mL)

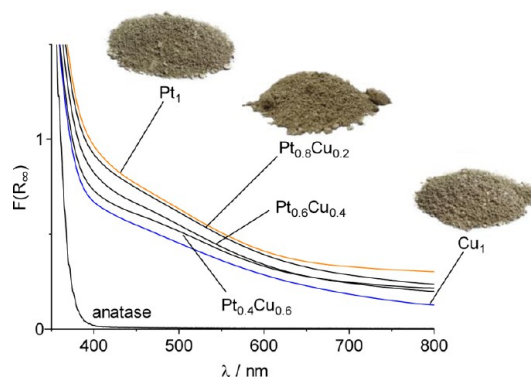


**Figure 2.** Diffuse-reflectance UV–vis spectra of  $\text{Pt}_{1-x}\text{Cu}_x$ /anatase (0.4 mol % of metal loading).

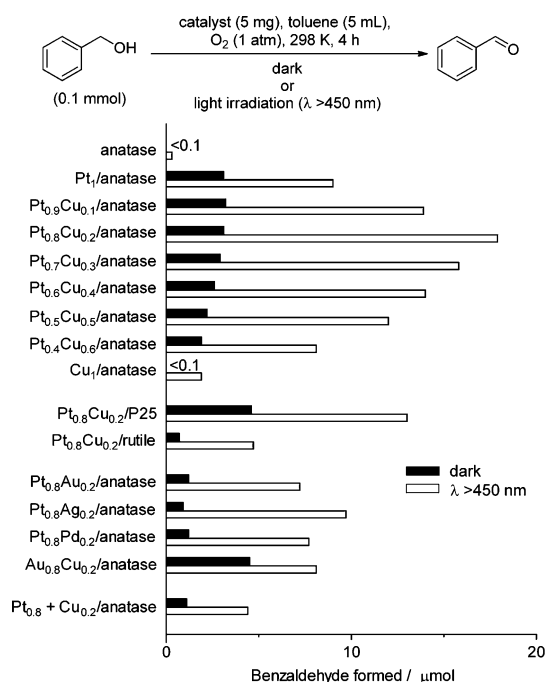


**Figure 3.** Amount of benzaldehyde formed by aerobic oxidation of benzyl alcohol with respective catalysts (0.4 mol % of metal loading), (black) in the dark, or (white) under irradiation of visible light ( $\lambda > 450$  nm; light intensity at 450–800 nm,  $16.8 \text{ mW cm}^{-2}$ ).

containing benzyl alcohol (0.1 mmol) and catalyst (5 mg) with  $\text{O}_2$  (1 atm). The temperature of the solution was kept continuously at  $298 \pm 0.5$  K by a digitally controlled water bath. Figure 3 summarizes the amount of benzaldehyde produced by 4 h reaction with respective catalysts in the dark or visible light irradiation by a Xe lamp ( $\lambda > 450$  nm). It is noted that both reactions selectively produce benzaldehyde (mass balance: >99%). In the dark (black), bare anatase promotes almost no reaction, but  $\text{Pt}_1$ /anatase produces  $3 \mu\text{mol}$  of benzaldehyde due to the catalytic activity of Pt particles.<sup>35,36</sup> The increase in Cu amount decreases the activity, and  $\text{Cu}_1$ /anatase promotes almost no reaction. Visible light irradiation enhances the activity (white):  $\text{Pt}_1$ /anatase produces  $9 \mu\text{mol}$  of

benzaldehyde, which is 3 times that obtained in the dark. Alloy catalysts further enhance activity; Pt<sub>0.8</sub>Cu<sub>0.2</sub>/anatase produces the largest amount of benzaldehyde (18  $\mu$ mol), which is twice that obtained with Pt<sub>1</sub>/anatase (9  $\mu$ mol). Further Cu alloying, however, decreases the activity, and Cu<sub>1</sub>/anatase shows almost no activity. These data suggest that the alloy catalyst with a small amount of Cu promotes efficient aerobic oxidation under visible light irradiation. In addition, as shown in Figure S4 (Supporting Information), the Pt<sub>0.8</sub>Cu<sub>0.2</sub>/anatase catalyst maintains its activity even after prolonged photoirradiation ( $\sim$ 24 h), indicating that the catalyst is stable under photoirradiation.

Anatase TiO<sub>2</sub> is necessary as the support. As shown in Figure 3 (Pt<sub>0.8</sub>Cu<sub>0.2</sub>/P25), visible light irradiation of the Pt<sub>0.8</sub>Cu<sub>0.2</sub> alloy loaded on P25 (a mixture of anatase and rutile TiO<sub>2</sub>) also enhances activity, but the enhancement is lower than that of Pt<sub>0.8</sub>Cu<sub>0.2</sub>/anatase. In addition, Pt<sub>0.8</sub>Cu<sub>0.2</sub>/rutile shows much lower activity. These data suggest that Pt–Cu alloy particles loaded on anatase TiO<sub>2</sub> exhibit very high activity, as also observed for monometallic Pt/anatase system.<sup>19</sup> It must also be noted that (Figure 3) Pt–Au,<sup>37</sup> Pt–Ag,<sup>38</sup> Pt–Pd,<sup>39</sup> and Au–Cu<sup>40</sup> alloy particles, often used for aerobic oxidation, show activity much lower than that of the Pt–Cu alloy. In addition, the Pt<sub>0.8</sub> + Cu<sub>0.2</sub>/anatase catalyst, prepared by a step-by-step deposition of respective Pt and Cu metals onto the anatase surface, scarcely exhibits reaction enhancement by visible light irradiation. These data clearly suggest that homogeneously mixed Pt–Cu alloy particles loaded on anatase TiO<sub>2</sub> are necessary for efficient aerobic oxidation under visible light.

**Mechanism for Reaction Enhancement.** In the PtCu/anatase system, photoactivated alloy particles efficiently transfer e<sup>−</sup> to anatase. This enhances the reduction of O<sub>2</sub> by e<sup>−</sup> on the anatase surface, resulting in enhanced aerobic oxidation. The enhanced e<sup>−</sup> transfer from the alloy particles to anatase is confirmed by electron spin resonance (ESR) analysis of the catalysts. Figure 4a (black) shows the ESR spectra of Pt<sub>0.8</sub>Cu<sub>0.2</sub>/anatase measured in the dark at 77 K after exposure to O<sub>2</sub>. Two signals observed at  $g = 2.001$  and 2.029 are assigned to O<sup>−</sup> produced by dissociative adsorption of O<sub>2</sub> onto the oxygen vacancy sites of the TiO<sub>2</sub> surface.<sup>41</sup> As shown by the blue line in Figure 4a, visible light irradiation of the sample creates strong signals assigned to superoxide anion stabilized on the TiO<sub>2</sub> surface (O<sub>2</sub><sup>−</sup>;  $g_{xx} = 2.002$ ,  $g_{yy} = 2.009$ ,  $g_{zzI} = 2.028$ ,  $g_{zzII} = 2.033$ ,  $g_{zzIII} = 2.038$ , and  $g_{zzIV} = 2.052$ ).<sup>42</sup> This indicates that visible light irradiation of alloy nanoparticles indeed transfers their e<sup>−</sup> to anatase, and the e<sup>−</sup> reduces O<sub>2</sub> on the anatase surface. As shown in Figure 4b, Pt<sub>1</sub>/anatase catalyst also exhibits an O<sub>2</sub><sup>−</sup> signal by visible light irradiation, but the signal intensity is much lower than that obtained on the alloy catalyst. These data suggest that photoactivated PtCu alloy particles

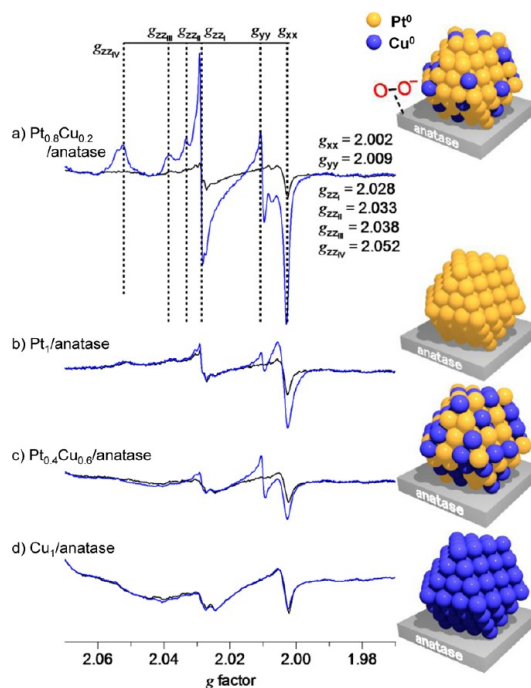


**Figure 4.** ESR spectra of (a) Pt<sub>0.8</sub>Cu<sub>0.2</sub>/anatase, (b) Pt<sub>1</sub>/anatase, (c) Pt<sub>0.4</sub>Cu<sub>0.6</sub>/anatase, and (d) Cu<sub>1</sub>/anatase measured at 77 K. The respective samples were treated with O<sub>2</sub> (20 Torr) for 3 h in the dark at 298 K (black). The samples were irradiated by visible light for 3 h at 298 K (blue). The metal loading of the catalysts is 0.4 mol %.

transfer their e<sup>−</sup> to anatase more efficiently than the monometallic Pt particles.

The efficiency for e<sup>−</sup> transfer from photoactivated nanoparticles to anatase depends on the Pt/Cu ratio of alloy particles. As shown in Figure 4c, visible light irradiation of Pt<sub>0.4</sub>Cu<sub>0.6</sub>/anatase with O<sub>2</sub> shows O<sub>2</sub><sup>−</sup> signals much weaker than that formed on Pt<sub>0.8</sub>Cu<sub>0.2</sub>/anatase (Figure 4a). In addition, as shown in Figure 4d, Cu<sub>1</sub>/anatase shows almost no O<sub>2</sub><sup>−</sup> signal. The intensity of the O<sub>2</sub><sup>−</sup> signal on the respective catalysts (Figure 4a–d) is consistent with the catalytic activity under visible light irradiation (Figure 3). These data suggest that the e<sup>−</sup> transfer from photoactivated nanoparticles to anatase is the crucial factor controlling the photocatalytic activity. The Pt<sub>0.8</sub>Cu<sub>0.2</sub>/anatase catalyst efficiently promotes e<sup>−</sup> transfer and exhibits very high activity.

Figure 5 (black) shows the action spectrum for aerobic oxidation of benzyl alcohol with Pt<sub>0.8</sub>Cu<sub>0.2</sub>/anatase obtained by irradiation of monochromatic light. A good correlation is observed between the interband absorption of the catalyst and the apparent quantum yield for benzaldehyde formation ( $\Phi_{AQY}$ ). This suggests that, as shown in Scheme 1, the interband excitation of alloy particles by visible light indeed promotes aerobic oxidation. It is also noted that  $\Phi_{AQY}$  for Pt<sub>0.8</sub>Cu<sub>0.2</sub>/anatase is much higher than that for Pt<sub>1</sub>/anatase (white); the  $\Phi_{AQY}$  for Pt<sub>0.8</sub>Cu<sub>0.2</sub>/anatase determined at 550 nm (17%) is more than twice that for Pt<sub>1</sub>/anatase (7.1%).

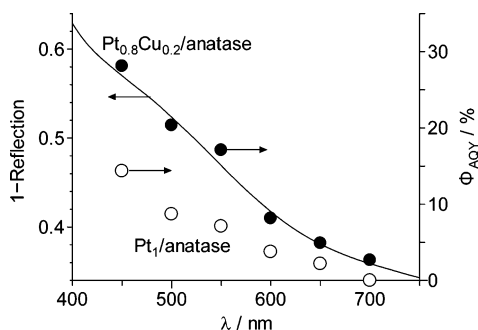


**Figure 5.** Action spectra for aerobic oxidation of benzyl alcohol on the  $\text{Pt}_{0.8}\text{Cu}_{0.2}/\text{anatase}$  and  $\text{Pt}_1/\text{anatase}$  catalysts (0.4 mol % of metal loading). The apparent quantum yield for benzaldehyde formation ( $\Phi_{\text{AQY}}$ ) was calculated with the equation  $\Phi_{\text{AQY}} (\%) = [(Y_{\text{vis}} - Y_{\text{dark}}) \times 2] / (\text{photon number entered into the reaction vessel}) \times 100$ , where  $Y_{\text{vis}}$  and  $Y_{\text{dark}}$  are the amounts of benzaldehyde formed ( $\mu\text{mol}$ ) under light irradiation and dark conditions, respectively.

As shown in Scheme 1, visible light absorption of Pt promotes interband transition of  $e^-$  from the 5d band to the sp conduction band.<sup>18</sup> The  $e^-$  is transferred to the anatase conduction band, where the  $e^-$  overcomes the Schottky barrier ( $\phi_B$ ) created at the heterojunction.<sup>21</sup> The enhanced  $e^-$  transfer from photoactivated alloy particles to anatase is due to the decrease in the height of  $\phi_B$  by Cu alloying. As shown by eq 1,  $\phi_B$  is defined as the difference between the work function of alloy particles and the electron affinity of the anatase conduction band.<sup>22</sup> The work function of the bimetallic alloy is expressed by the sum of the work functions of two metal components.<sup>23,24</sup> The work function of bulk  $\text{Pt}_{1-x}\text{Cu}_x$  alloy ( $W_{\text{alloy}\infty}$ ) is expressed as follows:

$$W_{\text{alloy}\infty} (\text{eV}) = (1 - x) \times W_{\text{Pt}\infty} + x \times W_{\text{Cu}\infty} \quad (2)$$

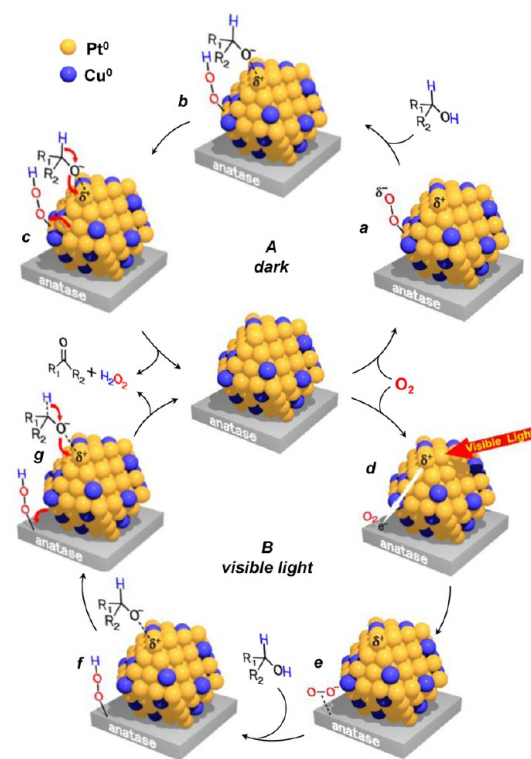
$W_{\text{Pt}\infty}$  and  $W_{\text{Cu}\infty}$  are the work functions of bulk Pt (5.65 eV) and Cu (4.65 eV),<sup>43</sup> respectively.  $W_{\text{alloy}\infty}$  for the bulk  $\text{Pt}_{0.8}\text{Cu}_{0.2}$  alloy is therefore calculated to be 5.45 eV. As reported,<sup>44</sup> the work function of metal particles depends on their size ( $d$ ). The work function of alloy particles ( $W_{\text{alloy}}$ ) is expressed as follows:

$$W_{\text{alloy}} (\text{eV}) = W_{\text{alloy}\infty} + \frac{1.08}{d} \quad (3)$$

The average diameters of nanoparticles on  $\text{Pt}_1/\text{anatase}$  and  $\text{Pt}_{0.8}\text{Cu}_{0.2}/\text{anatase}$  are determined by TEM observations to be 3.3 and 3.4 nm, respectively. The  $W_{\text{alloy}}$  values for the nanoparticles on these catalysts are therefore calculated to be 5.98 and 5.77 eV, respectively. Smaller work function of the alloy particles indicates that alloying of Cu possessing a smaller work function decreases the height of  $\phi_B$ . This thus promotes efficient  $e^-$  transfer to anatase and results in higher photocatalytic activity of  $\text{Pt}_{0.8}\text{Cu}_{0.2}/\text{anatase}$ . At the metal/semiconductor heterojunction, Fermi level pinning usually occurs and makes the Schottky barrier height less sensitive to the work function of metal loaded.<sup>45</sup> It is, however, well-known that the pinning

effect depends on the type and size of semiconductors. In particular, the size of  $\text{TiO}_2$  particles strongly affects the pinning effect:<sup>46,47</sup> the effect scarcely occurs on the  $\text{TiO}_2$  particles with small diameter ( $\sim 60$  nm) due to the high electronegativity of the Ti–O bond. The  $\text{TiO}_2$  particles used in the present work are very small (average diameter, 21.1 nm). This implies that the Fermi level pinning may scarcely occur on the present system. This therefore results in a decrease in the height of  $\phi_B$  by the Cu alloying, thus facilitating the enhanced  $e^-$  transfer from photoactivated alloy nanoparticles to anatase on the  $\text{Pt}_{0.8}\text{Cu}_{0.2}/\text{anatase}$  catalyst. In contrast, further increase in the Cu amount of nanoparticles would decrease the height of  $\phi_B$  more significantly. In this case, interband excitation of 5d  $e^-$  of Pt atoms is suppressed due to the decrease in Pt amount. This results in decreased efficiency for  $e^-$  transfer to anatase (Figure 4d) and decreases photocatalytic activity (Figure 3).

The reaction mechanism on the PtCu/anatase catalyst is explained as Scheme 2. As shown in Scheme 2A, the dark reaction is initiated by activation of  $\text{O}_2$  on the anionic Pt site (a).<sup>48</sup> The activated species removes the H atom from alcohol and produces hydroperoxide and alcoholate species on the surface (b).<sup>49</sup> Subsequent removal of the H atom from alcoholate species affords the product (c). Under irradiation of visible light (Scheme 2B), photoactivated alloy particles transfer  $e^-$  to anatase (d). In that, the height of the Schottky



**Scheme 2.** Proposed mechanism for aerobic oxidation of alcohol on the alloy catalyst (A) in the dark and (B) under visible light.

barrier created at the interface is decreased by Cu alloying, thus promoting efficient  $e^-$  transfer. The  $e^-$  reduces  $O_2$  and produces  $O_2^-$  species on the anatase surface (e). The  $O_2^-$  attracts the H atom from alcohol and produces the hydroperoxide and alcoholate species (f), giving rise to the product (g).

**Effect of the Amount of Metal Loaded.** The activity of  $Pt_{0.8}Cu_{0.2}$ /anatase depends on the amount of metal loaded. This is confirmed by aerobic oxidation using the  $Pt_{0.8}Cu_{0.2}$ /anatase catalysts with different metal loadings [(Pt + Cu)/anatase  $\times$  100 = 0.2–2.4 mol %]. As shown in Figure 6a (orange), the particle sizes ( $d$ ) of these catalysts are similar (3.4–3.6 nm), although the absorbance of catalysts in the visible region increases with the metal loadings (Figure 7a). The bar graphs in Figure 6a shows the results for aerobic oxidation of benzyl alcohol with respective catalysts. The dark activity (black) increases with the metal loadings due to the increase in the number of surface Pt atoms, active for aerobic oxidation.<sup>50,51</sup> Visible light irradiation (white) further enhances the reaction. The activity enhancement for the catalyst with 0.2 mol % of  $Pt_{0.8}Cu_{0.2}$  alloy is low, but that for the catalysts with >0.4 mol % of  $Pt_{0.8}Cu_{0.2}$  alloy is similar. This means that the >0.4 mol % of metal loadings scarcely affects the

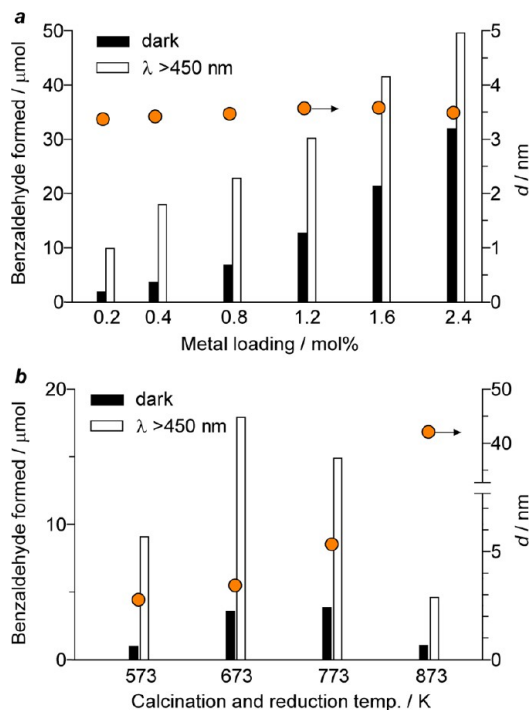


**Figure 6.** Effect of the (a) amount of  $Pt_{0.8}Cu_{0.2}$  alloy particles loaded and (b) calcination and reduction temperature on the amount of benzaldehyde formed during aerobic oxidation of benzyl alcohol with  $Pt_{0.8}Cu_{0.2}$ /anatase catalysts, (black) in the dark, and (white) under visible light irradiation. Orange keys denote the size of  $Pt_{0.8}Cu_{0.2}$  alloy particles ( $d$ ) on the catalysts. The calcination and reduction temperature employed for catalysts (a) is 673 K, and the metal loading of the catalysts (b) is 0.4 mol %. Reaction conditions are identical to those in Figure 3.

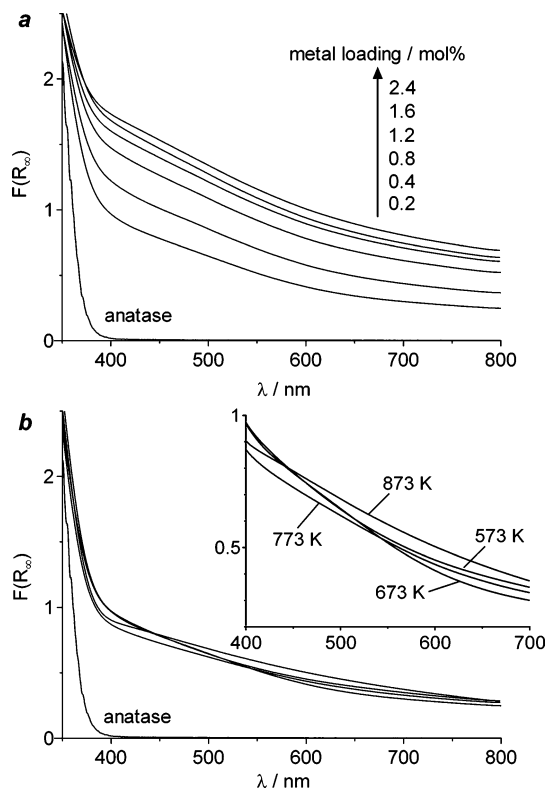


**Figure 7.** Diffuse-reflectance UV–vis spectra of (a)  $Pt_{0.8}Cu_{0.2}$ /anatase catalysts with different metal loadings prepared at 673 K and (b)  $Pt_{0.8}Cu_{0.2}$ /anatase catalysts with 0.4 mol % of metal loading prepared at different calcination and reduction temperature.

activity enhancement by visible light irradiation, although a larger number of alloy nanoparticles are loaded on the surface. As reported,<sup>52</sup> the increase in the amount of metal loaded onto the semiconductor leads to an increase in  $\phi_B$ , due to the decrease in the Fermi level of the semiconductor. The  $\phi_B$  increase probably suppresses  $e^-$  transfer from photoactivated nanoparticles to anatase, resulting in almost similar photocatalytic activity.

**Effect of Particle Size.** The size of  $Pt_{0.8}Cu_{0.2}$  alloy particles ( $d$ ) also affects the photocatalytic activity. The  $Pt_{0.8}Cu_{0.2}$ /anatase catalysts were prepared at different calcination and reduction temperatures (573–873 K) while maintaining 0.4 mol % of metal loading. As shown in Figure 6b (orange),  $d$  of the catalysts increases with a rise in temperature due to the sintering of nanoparticles; the treatment at 573, 673, 773, and 873 K creates metal particles with 2.8, 3.4, 5.3, and 42 nm diameters, respectively. X-ray diffraction (XRD) pattern of the catalysts (Figure S5; Supporting Information) indicates that the anatase-to-rutile phase transition scarcely occurs. In addition, dynamic laser scattering analysis of the catalysts revealed that the size of these catalysts is 22.4 nm (573 K), 23.8 nm (673 K), 23.9 nm (773 K), and 24.2 nm (873 K), respectively. This means that the size of anatase support is almost similar, although the size of alloy nanoparticles

increases with a rise in temperature. As shown by the black bars in Figure 6b, in the dark conditions, the catalysts prepared at 673 and 773 K show relatively high activity, and the catalysts with smaller or larger particles show lower activity. The lower activity of smaller particles is due to the decreased density of low-coordination sites that are active for oxidation.<sup>53</sup> In contrast, larger particles contain a decreased number of surface Pt atoms and, hence, show decreased activity.

As shown by the white bars (Figure 6b), photocatalytic activity of Pt<sub>0.8</sub>Cu<sub>0.2</sub>/anatase prepared at different calcination and reduction temperature shows *d* dependence similar to the dark activity. The catalyst prepared at 673 K shows the highest activity, and the catalysts with smaller or larger particles show decreased activity. As shown in Figure 7b, absorbance of the catalysts in the visible region is similar, although their *d* values are different (Figure 6b). This indicates that the light absorption efficiencies for these catalysts are similar. The low activity of the catalysts with smaller Pt particles is due to the height of  $\phi_B$  created at the nanoparticle/anatase interface. As shown by eq 3, the work function of metal particles increases with a decrease in their particle size. The *d* values for the catalysts prepared at 573, 673, 773, and 873 K are 2.8, 3.4, 5.3, and 42 nm, respectively, and their  $W_{\text{alloy}}$  values are calculated to be 5.84, 5.77, 5.65, and 5.48 eV, respectively. As summarized in Figure 8 (black), the  $W_{\text{alloy}}$  values become more positive with a decrease in the particle size. This suggests that the catalysts with smaller Pt particles create higher  $\phi_B$ . This may suppress smooth  $e^-$  transfer from photoactivated alloy particles to anatase, thus resulting in decreased photocatalytic activity (Figure 6b).

In contrast, larger alloy particles create lower  $\phi_B$  due to their lower work function; therefore, the  $e^-$  transfer to anatase would occur more easily. However, as shown in Figure 6b, photocatalytic activity of the

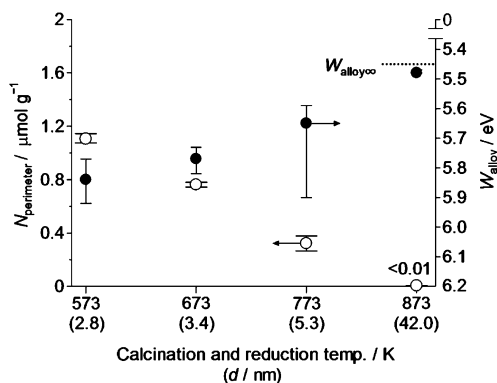
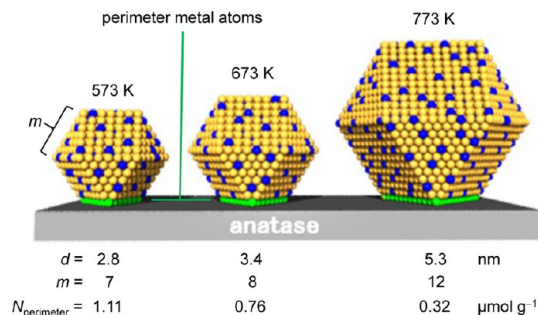


**Figure 8.** (Black) Work function of Pt<sub>0.8</sub>Cu<sub>0.2</sub> alloy particles ( $W_{\text{alloy}}$ ) and (white) the number of perimeter metal atoms ( $N_{\text{perimeter}}$ ) for Pt<sub>0.8</sub>Cu<sub>0.2</sub>/anatase catalysts with 0.4 mol % of metal loading prepared at different calcination and reduction temperature. The detailed calculation results for  $N_{\text{perimeter}}$  are summarized in Table S1 (Supporting Information).



**Scheme 3.** Relationship between the size of metal particles and the number of perimeter metal atoms on Pt<sub>0.8</sub>Cu<sub>0.2</sub>/anatase catalysts prepared at different calcination and reduction temperature.

catalysts with larger alloy particles is much lower than that prepared at 673 K. As shown in Scheme 3, the  $e^-$  transfer from photoactivated metal particles to anatase occurs through the perimeter atoms indicated by the green spheres.<sup>19</sup> The number of perimeter metal atoms may therefore affect the  $e^-$  transfer efficiency. As shown in Figure 1c–h, the high-resolution TEM images of catalysts revealed that the shape of many alloy particles is a part of a cuboctahedron, which is surrounded by (111) and (100) surfaces. The PtCu alloy particles on the anatase surface therefore can simply be modeled as a fcc cuboctahedron,<sup>54</sup> as often used for related systems.<sup>55,56</sup> This thus allows rough determination of the number of perimeter metal atoms. Considering the full shell close-packing cuboctahedron for the PtCu alloy particle, where one atom is surrounded by 12 others, the number of total metal atoms per particle ( $N_{\text{total}}^*$ ) can be expressed by eq 4 using the number of shells (*m*).  $N_{\text{total}}^*$  is rewritten with the average diameter of alloy particle (*d*) and the average atomic diameter of Pt and Cu [ $d_{\text{atom}} (= 0.274 \text{ nm}) = 0.8 \times d_{\text{atom,Pt}} (= 0.278 \text{ nm}) + 0.2 \times d_{\text{atom,Cu}} (= 0.256 \text{ nm})$ ].<sup>57</sup> The number of perimeter metal atoms per particle ( $N_{\text{perimeter}}^*$ ) is expressed by eq 5.<sup>54</sup>

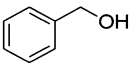
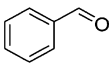
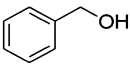
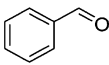
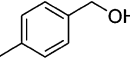
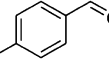
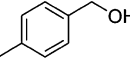
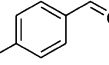
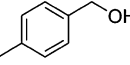
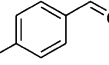
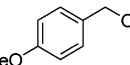
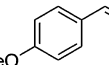
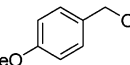
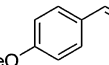
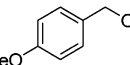
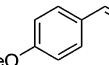
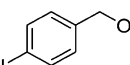
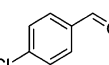
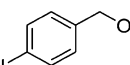
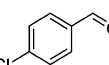
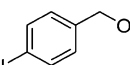
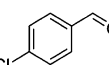
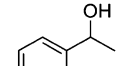
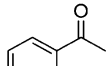
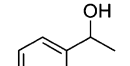
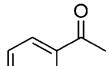
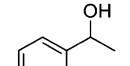
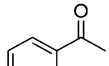
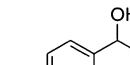
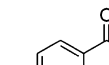
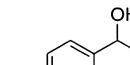
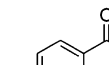
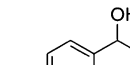
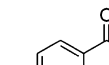
$$N_{\text{total}}^*(-) = \frac{10m^3 - 15m^2 + 11m - 3}{3} = \left( \frac{d}{1.105 \times d_{\text{atom}}} \right)^3 \quad (4)$$

$$N_{\text{perimeter}}^*(-) = 3m - 3 \quad (5)$$

The number of alloy particles per gram catalyst ( $N_{\text{particle}}$ ) is expressed by eq 6, using the percent amount of metal loaded [0.87 wt % = (Pt + Cu)/(Pt + Cu + anatase) × 100], average molecular weight of Pt and Cu [ $M_W (= 168.8 \text{ g mol}^{-1}) = 0.8 \times M_{\text{Pt}} (= 195.1 \text{ g mol}^{-1}) + 0.2 \times M_{\text{Cu}} (= 63.5 \text{ g mol}^{-1})$ ], and  $N_{\text{total}}^*$ . The number of perimeter metal atoms per gram catalyst ( $N_{\text{perimeter}}$ ) is therefore expressed by eq 7.

$$N_{\text{particle}} (\text{mol g}^{-1}) = \frac{0.87}{100 \times M_W \times N_{\text{total}}^*} \quad (6)$$

TABLE 1. Effect of Sunlight Exposure on Aerobic Oxidation of Alcohols<sup>a</sup>

entry	substrate	catalyst	sunlight <sup>b</sup>	conv / % <sup>c</sup>	product	yield / % <sup>d</sup>
1		Pt <sub>0.8</sub> Cu <sub>0.2</sub> /anatase	+	75		72
2		Pt <sub>0.8</sub> Cu <sub>0.2</sub> /anatase	–	13		12
3		Pt <sub>1</sub> /anatase	+	37		35
4		Pt <sub>0.8</sub> Cu <sub>0.2</sub> /anatase	+	84		80
5		Pt <sub>0.8</sub> Cu <sub>0.2</sub> /anatase	–	9		9
6		Pt <sub>1</sub> /anatase	+	60		59
7		Pt <sub>0.8</sub> Cu <sub>0.2</sub> /anatase	+	>99		99
8		Pt <sub>0.8</sub> Cu <sub>0.2</sub> /anatase	–	14		14
9		Pt <sub>1</sub> /anatase	+	77		77
10		Pt <sub>0.8</sub> Cu <sub>0.2</sub> /anatase	+	73		73
11		Pt <sub>0.8</sub> Cu <sub>0.2</sub> /anatase	–	7		7
12		Pt <sub>1</sub> /anatase	+	43		40
13		Pt <sub>0.8</sub> Cu <sub>0.2</sub> /anatase	+	72		72
14		Pt <sub>0.8</sub> Cu <sub>0.2</sub> /anatase	–	11		10
15		Pt <sub>1</sub> /anatase	+	34		34
16		Pt <sub>0.8</sub> Cu <sub>0.2</sub> /anatase	+	85		84
17		Pt <sub>0.8</sub> Cu <sub>0.2</sub> /anatase	–	5		5
18		Pt <sub>1</sub> /anatase	+	49		49

<sup>a</sup> Reaction conditions: toluene (5 mL), alcohol (25  $\mu$ mol), catalyst (5 mg), metal loading of catalysts (0.4 mol %), O<sub>2</sub> (1 atm), exposure time (4 h). The average light intensity at 300–800 nm was 4.6 mW cm<sup>-2</sup>, which involves  $\lambda < 400$  nm light with only  $\sim 2\%$  (Figure S6, Supporting Information). The solution temperature during exposure was 288–293 K. <sup>b</sup> The dark reaction (–) was performed at 293 K. <sup>c</sup> (Alcohol converted)/(initial amount of alcohol)  $\times$  100. <sup>d</sup> (Product formed)/(initial amount of alcohol)  $\times$  100.

$$N_{\text{perimeter}}(\text{mol g}^{-1}) = N_{\text{perimeter}}^* \times N_{\text{particle}} \quad (7)$$

The  $N_{\text{perimeter}}$  values for respective Pt<sub>0.8</sub>Cu<sub>0.2</sub>/anatase catalysts prepared at different temperature can therefore be calculated using their  $d$  values determined by TEM observations (Table S1, Supporting Information). As shown in Figure 8 (white),  $N_{\text{perimeter}}$  decreases with an increase in the particle size; the value for the catalyst prepared at 573 K is 1.1  $\mu$ mol g<sup>-1</sup>, but the value for the catalyst prepared at 873 K is only  $5.3 \times 10^{-3}$   $\mu$ mol g<sup>-1</sup>. This suggests that the particle size increase significantly decreases  $N_{\text{perimeter}}$ . This may suppress e<sup>-</sup> transfer from photoactivated alloy particles to anatase, resulting in low photocatalytic activity. As shown in Figure 6b, the catalysts prepared at 573, 673, and 773 K contain alloy particles with similar diameter (2–6 nm), but the catalyst prepared at 673 K shows the highest photocatalytic activity. This means that the particle size

strongly affects  $W_{\text{alloy}}$  and  $N_{\text{perimeter}}$  values, and this trade-off relationship is critical for activity. The 3–5 nm Pt<sub>0.8</sub>Cu<sub>0.2</sub> alloy nanoparticles with shell number 7–11 create relatively low  $\phi_B$  and large number of perimeter metal atoms at the nanoparticle/anatase heterojunction and, hence, exhibit high photocatalytic activity.

**Effect of Sunlight As the Light Source.** The Pt<sub>0.8</sub>Cu<sub>0.2</sub>/anatase catalyst prepared at 673 K successfully promotes aerobic oxidation of alcohols under sunlight irradiation at ambient temperature. Table 1 summarizes the results for oxidation of various alcohols obtained with Pt<sub>0.8</sub>Cu<sub>0.2</sub>/anatase under sunlight exposure, where the temperature of solution during exposure was 288–293 K. Sunlight irradiation selectively oxidizes alcohols to the corresponding carbonyl compounds with very high yields (75–99%). These yields are much higher than those obtained with



Pt<sub>0.8</sub>Cu<sub>0.2</sub>/anatase in the dark or with Pt<sub>1</sub>/anatase under sunlight exposure. These data suggest that the PtCu/anatase catalyst is successfully activated by sunlight and acts as an efficient photocatalyst.

## CONCLUSION

We found that bimetallic alloy nanoparticles consisting of 80 mol % of Pt and 20 mol % of Cu, supported on anatase TiO<sub>2</sub>, behave as highly efficient photocatalysts for aerobic oxidation under visible light irradiation. The activity of the alloy catalyst is much higher than that of the monometallic Pt catalyst. The enhanced activity is due to the decrease in the work function of nanoparticles by Cu alloying. This decreases the height of the Schottky barrier created at the nanoparticle/anatase heterojunction and promotes smooth e<sup>-</sup> transfer from the photoactivated nanoparticles

to anatase. The activity strongly depends on the size of alloy particles. Smaller particles (<3 nm diameter) have larger work function and create a larger Schottky barrier, resulting in decreased activity. In contrast, larger particles (>5 nm diameter) possess a smaller number of perimeter metal atoms. This thus suppresses smooth e<sup>-</sup> transfer from photoactivated nanoparticles to anatase, resulting in decreased activity. As a result of this, alloy nanoparticles with 3–5 nm diameters exhibit the highest photocatalytic activity. Sunlight activation of the catalyst successfully promotes selective and efficient oxidation of alcohols. The efficient charge separation at the Pt–Cu alloy nanoparticle/anatase interface clarified here may contribute to the creation of more active photocatalysts driven by visible light and the design of photocatalytic systems for selective organic transformation by sunlight.

## EXPERIMENTAL SECTION

**Materials.** All reagents used were purchased from Wako, Tokyo Kasei, and Sigma-Aldrich and used without further purification. Water was purified by the Milli-Q system. Anatase TiO<sub>2</sub> (JRC-TIO-1), P25 (JRC-TIO-4; average particle size, 24 nm; BET surface area, 57 m<sup>2</sup> g<sup>-1</sup>; anatase/rutile = ~83/17), and rutile TiO<sub>2</sub> (JRC-TIO-6; 15 nm; 104 m<sup>2</sup> g<sup>-1</sup>) were kindly supplied from the Catalyst Society of Japan.

**Pt<sub>1-x</sub>Cu<sub>x</sub>/TiO<sub>2</sub>.** These catalysts with 0.4 mol % of metal loading [ $x = \text{Cu}/(\text{Pt} + \text{Cu}) = 0, 0.1, 0.2, 0.3, 0.4, 0.5, 0.6, \text{ and } 1$ ] were prepared as follows. TiO<sub>2</sub> (1.0 g) and H<sub>2</sub>PtCl<sub>6</sub>·6H<sub>2</sub>O/Cu(NO<sub>3</sub>)<sub>2</sub>·3H<sub>2</sub>O (26.8/0, 24.2/1.2, 21.4/2.4, 9.4/3.6, 8.1/4.8, 6.7/6.1, 5.3/7.2, and 0/12.2 mg) were added to water (40 mL), and the solvent was evaporated with vigorous stirring at 353 K for 12 h. The resultant mixture was calcined under air flow and reduced with H<sub>2</sub> flow at the identical temperature. The temperature employed for calcination and reduction was 673 K unless otherwise noted. The heating rate and holding time for these treatments were 2 K min<sup>-1</sup> and 2 h, respectively.

**Pt<sub>0.8</sub> + Cu<sub>0.2</sub>/Anatase.** The catalyst with 0.4 mol % of metal loading was prepared by a step-by-step method as follows: Anatase TiO<sub>2</sub> (1.0 g) and H<sub>2</sub>PtCl<sub>6</sub>·6H<sub>2</sub>O (21.4 mg) were added to water (40 mL), and the solvent was evaporated with vigorous stirring at 353 K for 3 h. The particles were recovered by centrifugation, washed with water, and dried at 353 K for 12 h. The powders were calcined at 673 K for 2 h under air flow and reduced at 673 K for 2 h under H<sub>2</sub> flow. The obtained powder and Cu(NO<sub>3</sub>)<sub>2</sub>·3H<sub>2</sub>O (2.4 mg) were added to water (40 mL), and solvent was evaporated with vigorous stirring at 353 K for 12 h. The resultant mixture was calcined at 673 K for 2 h under air flow and reduced at 673 K for 2 h under H<sub>2</sub> flow.

**Pt<sub>0.8</sub>M<sub>0.2</sub>/Anatase (M = Au, Ag, Pd).** These catalysts with 0.4 mol % of metal loading were prepared as follows: Anatase TiO<sub>2</sub> (1.0 g) and H<sub>2</sub>PtCl<sub>6</sub>·6H<sub>2</sub>O/HAuCl<sub>4</sub>·4H<sub>2</sub>O (21.4/4.2 mg), H<sub>2</sub>PtCl<sub>6</sub>·6H<sub>2</sub>O/AgNO<sub>3</sub> (21.4/1.7 mg), or H<sub>2</sub>PtCl<sub>6</sub>·6H<sub>2</sub>O/Pd(NO<sub>3</sub>)<sub>2</sub> (21.4/2.3 mg) were added to water (40 mL), and solvent was evaporated with vigorous stirring at 353 K for 12 h. The resultant mixture was calcined at 673 K for 2 h in air and reduced at 673 K for 2 h with H<sub>2</sub>.

**Au<sub>0.8</sub>Cu<sub>0.2</sub>/Anatase.** This catalyst with 0.4 mol % metal loading was prepared according to the procedure described previously.<sup>40</sup> Anatase TiO<sub>2</sub> (1.0 g) was added to water (100 mL) containing HAuCl<sub>4</sub>·4H<sub>2</sub>O (16.8 mg) and Cu(NO<sub>3</sub>)<sub>2</sub>·3H<sub>2</sub>O (2.6 mg). The pH of solution was adjusted to ~7 with 1 mM NaOH, and the solution was stirred at 353 K for 3 h. The particles were recovered by centrifugation, washed thoroughly with water, and dried at 353 K for 12 h. The obtained powders were reduced at 673 K under H<sub>2</sub> flow. The heating rate was 2 K min<sup>-1</sup>, and the temperature was kept at 673 K for 2 h.

**Reaction Procedure.** Catalyst (5 mg) was added to toluene (5 mL) containing an alcohol within a Pyrex glass tube ( $\varphi$  12 mm; capacity, 20 mL). The tube was sealed with a rubber septum cap. The catalyst was dispersed well by ultrasonication for 5 min, and O<sub>2</sub> was bubbled through the solution for 5 min. The tube was immersed in a temperature-controlled water bath (298 ± 0.5 K). The tube was photoirradiated with magnetic stirring using a 2 kW Xe lamp (USHIO Inc.) and filtered through a glass filter (CS3-72; Kopp Glass Inc.) to give light wavelength of  $\lambda > 450$  nm, where the light intensity at 450–800 nm was 16.8 mW cm<sup>-2</sup>. Sunlight reactions were performed on December, 4, 2012 at 10:00–14:00 at the top of the laboratory building (latitude 34.7° north, longitude 135.5° east). The light intensity at 300–800 nm was 4.6 mW cm<sup>-2</sup>. The highest temperature during reaction was 293 K, and the dark reactions were performed at 293 K. After the reaction, the catalyst was recovered by centrifugation. The liquid-phase products were analyzed by GC-FID (Shimadzu, GC-2040).

**Action Spectrum Analysis.** Catalyst (8 mg) was suspended in toluene (2 mL) containing benzyl alcohol (0.4 mmol) within a Pyrex glass tube ( $\varphi$  12 mm; capacity, 20 mL). The tube was sealed with a rubber septum cap. The catalyst was dispersed well by ultrasonication for 5 min, and O<sub>2</sub> was bubbled through the solution for 5 min. The solution was photoirradiated with 2 kW Xe lamp (USHIO Inc.), where the incident light was monochromated by band-pass glass filters (Asahi Techno Glass Co.). The full width at half-maximum (fwhm) of the monochromatic light was 11–16 nm. The temperature of solution during photoirradiation was kept at 298 ± 0.5 K with a temperature-controlled water bath. The photon number entered into the reaction vessel was determined with a spectroradiometer USR-40 (USHIO Inc.).

**ESR Measurement.** The spectra were recorded at the X-band using a Bruker EMX-10/12 spectrometer with a 100 kHz magnetic field modulation at a microwave power level of 10.0 mW,<sup>17</sup> where microwave power saturation of the signal does not occur. The magnetic field was calibrated with 1,1'-diphenyl-2-picrylhydrazyl (DPPH). Catalyst (20 mg) was placed in a quartz ESR tube and evacuated at 423 K for 3 h. After cooling the sample tube to room temperature, O<sub>2</sub> (20 Torr) was introduced to the tube and kept for 3 h at 298 K. The tube was photoirradiated for 1 h at 298 K using a Xe lamp (2 kW; USHIO Inc.) at  $\lambda > 450$  nm (with CS3-72; Kopp Glass Inc.). The ESR tube was then evacuated for 10 min to remove the excess amount of O<sub>2</sub> and subjected to analysis at 77 K.

**Analysis.** Total amounts of Pt and Cu in the catalysts were analyzed by an inductively coupled argon plasma atomic emission spectrometer (Seiko Instruments, Inc.; SPS7800), after

dissolution of the catalysts in an aqua regia. Diffuse-reflectance UV–vis spectra were measured on an UV–vis spectrophotometer (Jasco Corp.; V-550 with Integrated Sphere Apparatus ISV-469) with BaSO<sub>4</sub> as a reference. TEM observations were carried out using an FEI Tecnai G2 20ST analytical electron microscope operated at 200 kV, equipped with an energy-dispersive X-ray spectroscopy (EDX) detector.<sup>58</sup> EDX spectra from a metallic particle were taken under scanning transmission electron microscopy (STEM) mode. XPS measurements were performed using a JEOL JPS-9000MX spectrometer using Mg K $\alpha$  radiation as the energy source. XRD patterns were obtained on a Philips XXX diffractometer with Cu K $\alpha$  radiation. Hydrodynamic diameter of the catalysts was measured by a dynamic laser scattering spectrometer (LB-500, HORIBA).<sup>58</sup>

**Conflict of Interest:** The authors declare no competing financial interest.

**Acknowledgment.** This work was supported by the Grant-in-Aid for Scientific Research (No. 23360349) from the Ministry of Education, Culture, Sports, Science and Technology, Japan (MEXT).

**Supporting Information Available:** TEM images (Figure S1), XPS results (Figure S2), EDX results (Figure S3), time-dependent change in the amount of benzaldehyde formed during photo-reaction (Figure S4), XRD patterns (Figure S5), light emission spectra for Xe lamp and sunlight (Figure S6), and properties of the catalysts used (Table S1). This material is available free of charge via the Internet at <http://pubs.acs.org>.

## REFERENCES AND NOTES

- Sheldon, R. A.; Arends, I. W. C. E.; Dijkstra, A. New Developments in Catalytic Alcohol Oxidations for Fine Chemicals Synthesis. *Catal. Today* **2000**, *57*, 157–166.
- Fox, M. A.; Dulay, M. T. Heterogeneous Photocatalysis. *Chem. Rev.* **1993**, *93*, 341–357.
- Maldotti, A.; Molinari, A.; Amadelli, R. Photocatalysis with Organized Systems for the Oxofunctionalization of Hydrocarbons by O<sub>2</sub>. *Chem. Rev.* **2002**, *102*, 3811–3836.
- Palmisano, G.; Augugliaro, V.; Pagliano, M.; Palmisano, L. Photocatalysis: A Promising Route for 21st Century Organic Chemistry. *Chem. Commun.* **2007**, 3425–3437.
- Fagnoni, M.; Dondi, D.; Ravelli, D.; Albini, A. Photocatalysis for the Formation of the C–C Bond. *Chem. Rev.* **2007**, *107*, 2725–2756.
- Shiraishi, Y.; Hirai, T. Selective Organic Transformations on Titanium Oxide-Based Photocatalysts. *J. Photochem. Photobiol., C* **2008**, *9*, 157–170.
- Asahi, R.; Morikawa, T.; Ohwaki, T.; Aoki, T.; Taga, K. Y. Visible-Light Photocatalysis in Nitrogen-Doped Titanium Oxides. *Science* **2001**, *293*, 269–271.
- Miyauchi, M.; Ikezawa, A.; Tobimatsu, H.; Irie, H.; Hashimoto, K. Zeta Potential and Photocatalytic Activity of Nitrogen Doped TiO<sub>2</sub> Thin Films. *Phys. Chem. Chem. Phys.* **2004**, *6*, 865–870.
- Ohno, T.; Akiyoshi, M.; Umabayashi, T.; Asai, K.; Mitsui, T.; Matsumura, M. Preparation of S-Doped TiO<sub>2</sub> Photocatalysts and Their Photocatalytic Activities under Visible Light. *Appl. Catal., A* **2004**, *265*, 115–121.
- Yan, X.; Ohno, T.; Nishijima, K.; Abe, R.; Ohtani, B. Is Methylene Blue an Appropriate Substrate for a Photocatalytic Activity Test? A Study with Visible-Light Responsive Titania. *Chem. Phys. Lett.* **2006**, *429*, 606–610.
- Sakthivel, S.; Kisch, H. Daylight Photocatalysis by Carbon-Modified Titanium Dioxide. *Angew. Chem., Int. Ed.* **2003**, *42*, 4908–4911.
- Irie, H.; Watanabe, Y.; Hashimoto, K. Carbon-Doped Anatase TiO<sub>2</sub> Powders as a Visible-Light Sensitive Photocatalyst. *Chem. Lett.* **2003**, *32*, 772–773.
- Zhao, W.; Ma, W.; Chen, C.; Zhao, J.; Shuai, Z. Efficient Degradation of Toxic Organic Pollutants with Ni<sub>2</sub>O<sub>3</sub>/TiO<sub>2-x</sub>B<sub>x</sub> under Visible Irradiation. *J. Am. Chem. Soc.* **2004**, *126*, 4782–4783.
- Zaleska, A.; Sobczak, J. W.; Grabowska, E.; Hupka, J. Preparation and Photocatalytic Activity of Boron-Modified TiO<sub>2</sub> under UV and Visible Light. *Appl. Catal., B* **2008**, *78*, 92–100.
- Chen, X.; Mao, S. S. Titanium Dioxide Nanomaterials: Synthesis, Properties, Modifications, and Applications. *Chem. Rev.* **2007**, *107*, 2891–2959.
- Primo, A.; Corma, A.; García, H. Titania Supported Gold Nanoparticles as Photocatalyst. *Phys. Chem. Chem. Phys.* **2011**, *13*, 886–910.
- Tsukamoto, D.; Shiraishi, Y.; Sugano, Y.; Ichikawa, S.; Tanaka, S.; Hirai, T. Gold Nanoparticles Located at the Interface of Anatase/Rutile TiO<sub>2</sub> Particles as Active Plasmonic Photocatalysts for Aerobic Oxidation. *J. Am. Chem. Soc.* **2012**, *134*, 6309–6315.
- Hao, Q.; Juluri, B. K.; Zheng, Y. B.; Wang, B.; Chiang, I.-K.; Jensen, L.; Crespi, V.; Eklund, P. C.; Huang, T. J. Effects of Intrinsic Fano Interference on Surface Enhanced Raman Spectroscopy: Comparison between Platinum and Gold. *J. Phys. Chem. C* **2010**, *114*, 18059–18066.
- Shiraishi, Y.; Tsukamoto, D.; Sugano, Y.; Shiro, A.; Ichikawa, S.; Tanaka, S.; Hirai, T. Platinum Nanoparticles Supported on Anatase Titanium Dioxide as Highly Active Catalysts for Aerobic Oxidation under Visible Light Irradiation. *ACS Catal.* **2012**, *2*, 1984–1992.
- Gong, X.-Q.; Slloni, A.; Dulub, O.; Jacobson, P.; Diebold, U. Small Au and Pt Clusters at the Anatase TiO<sub>2</sub>(101) Surface: Behavior at Terraces, Steps, and Surface Oxygen Vacancies. *J. Am. Chem. Soc.* **2008**, *130*, 370–381.
- Schottky, W. Zur Halbleitertheorie der Sperrschicht- und Spitzengleichrichter. *Z. Phys.* **1939**, *113*, 367–414.
- Nakato, Y.; Ueda, K.; Yano, H.; Tsubomura, H. Effect of Microscopic Discontinuity of Metal Overlayers on the Photovoltages in Metal-Coated Semiconductor-Liquid Junction Photoelectrochemical Cells for Efficient Solar Energy Conversion. *J. Phys. Chem.* **1988**, *92*, 2316–2324.
- Pasti, I.; Mentus, S. Electronic Properties of the Pt<sub>x</sub>Me<sub>1-x</sub>/Pt(1 1 1) (Me = Au, Bi, In, Pb, Pd, Sn and Cu) Surface Alloys: DFT Study. *Mater. Chem. Phys.* **2009**, *116*, 94–101.
- Ishii, R.; Matsumura, K.; Sakai, A.; Sakata, T. Work Function of Binary Alloys. *Appl. Surf. Sci.* **2001**, *169–170*, 658–661.
- Shiraishi, Y.; Ikeda, M.; Tsukamoto, D.; Tanaka, S.; Hirai, T. One-Pot Synthesis of Imines from Alcohols and Amines with TiO<sub>2</sub> Loading Pt Nanoparticles under UV Irradiation. *Chem. Commun.* **2011**, *47*, 4811–4813.
- Shiraishi, Y.; Takeda, Y.; Sugano, Y.; Ichikawa, S.; Tanaka, S.; Hirai, T. Highly Efficient Photocatalytic Dehalogenation of Organic Halides on TiO<sub>2</sub> Loaded with Bimetallic Pd–Pt Alloy Nanoparticles. *Chem. Commun.* **2011**, *47*, 7863–7865.
- Li, L.; Xu, Z.; Liu, F.; Shao, Y.; Wang, J.; Wan, H.; Zheng, S. Photocatalytic Nitrate Reduction over Pt–Cu/TiO<sub>2</sub> Catalysts with Benzene as Hole Scavenger. *J. Photochem. Photobiol., A* **2010**, *212*, 113–121.
- Zhang, J.; Ma, J.; Wan, Y.; Jiang, J.; Zhao, X. S. Dendritic Pt–Cu Bimetallic Nanocrystals with a High Electrochemical Activity toward Methanol Oxidation. *Mater. Chem. Phys.* **2012**, *132*, 244–247.
- Kleiman, G. G.; Sundaram, V. S.; Rogers, J. D.; Moraes, M. B. X-ray Photoemission Spectroscopy of Pt–Cu: A Canonical Alloy. *Phys. Rev. B* **1981**, *23*, 3177–3185.
- Barrabés, N.; Frare, A.; Föttonger, K.; Urakawa, A.; Llorca, J.; Ruppel, G.; Tichit, D. Pt–Cu Bimetallic Catalysts Obtained from Layered Double Hydroxides by an Anion-Exchange Route. *Appl. Clay Sci.* **2012**, *69*, 1–10.
- Bigall, N. C.; Härtling, T.; Klose, M.; Simon, P.; Eng, L. M.; Eychmüller, A. Monodisperse Platinum Nanospheres with Adjustable Diameters from 10 to 100 nm: Synthesis and Distinct Optical Properties. *Nano Lett.* **2008**, *8*, 4588–4592.
- Desarkar, H. S.; Kumbhakar, P.; Mitra, A. K. Effect of Ablation Time and Laser Fluence on the Optical Properties of Copper Nano Colloids Prepared by Laser Ablation Technique. *Appl. Nanosci.* **2012**, *2*, 285–291.
- Pileni, M. P.; Lisiecki, I. Nanometer Metallic Copper Particle Synthesis in Reverse Micelles. *Colloids Surf., A* **1993**, *80*, 63–68.

34. Abad, A.; Corma, A.; Garcia, H. Catalyst Parameters Determining Activity and Selectivity of Supported Gold Nanoparticles for the Aerobic Oxidation of Alcohols: The Molecular Reaction Mechanism. *Chem.—Eur. J.* **2008**, *14*, 212–222.
35. Proch, S.; Herrmannsdörfer, J.; Kempe, R.; Kern, C.; Jess, A.; Seyfarth, L.; Senker, J. Pt@MOF-177: Synthesis, Room-Temperature Hydrogen Storage and Oxidation Catalysis. *Chem.—Eur. J.* **2008**, *14*, 8204–8212.
36. Ng, Y. H.; Ikeda, S.; Harada, T.; Morita, Y.; Matsumura, M. An Efficient and Reusable Carbon-Supported Platinum Catalyst for Aerobic Oxidation of Alcohols in Water. *Chem. Commun.* **2008**, 3181–3183.
37. Zhang, H.; Toshima, N. Synthesis of Au/Pt Bimetallic Nanoparticles with a Pt-Rich Shell and Their High Catalytic Activities for Aerobic Glucose Oxidation. *J. Colloid Interface Sci.* **2013**, *394*, 166–176.
38. Hwang, B. J.; Kumar, S. M. S.; Chen, C.-H.; Chang, R.-W.; Liu, D.-G.; Lee, J.-F. Size and Alloying Extent Dependent Physicochemical Properties of Pt–Ag/C Nanoparticles Synthesized by the Ethylene Glycol Method. *J. Phys. Chem. C* **2008**, *112*, 2370–2377.
39. Lapisardi, G.; Urfels, L.; Gélin, P.; Primet, M.; Kaddouri, A.; Garbowski, E.; Toppi, S.; Tena, E. Superior Catalytic Behaviour of Pt-Doped Pd Catalysts in the Complete Oxidation of Methane at Low Temperature. *Catal. Today* **2006**, *117*, 564–568.
40. Sugano, Y.; Shiraishi, Y.; Tsukamoto, D.; Ichikawa, S.; Tanaka, S.; Hirai, T. Supported Au–Cu Bimetallic Alloy Nanoparticles as Catalyst for Aerobic Oxidation with Regenerable Activity by Visible Light Irradiation. *Angew. Chem., Int. Ed.* **2013**, *52*, 5295–5299.
41. Coronado, J. M.; Soria, J. ESR Study of the Initial Stages of the Photocatalytic Oxidation of Toluene over TiO<sub>2</sub> Powders. *Catal. Today* **2007**, *123*, 37–41.
42. Anpo, M.; Che, M.; Fubini, B.; Garrone, E.; Giamello, E.; Paganini, M. C. Generation of Superoxide Ions at Oxide Surfaces. *Top. Catal.* **1999**, *8*, 189–198.
43. Eastman, D. E. Photoelectric Work Functions of Transition, Rare-Earth, and Noble Metals. *Phys. Rev. B.* **1970**, *2*, 1–2.
44. Wood, D. M. Classical Size Dependence of the Work Function of Small Metallic Spheres. *Phys. Rev. Lett.* **1981**, *46*, 749–749.
45. Bardeen, J. Surface States and Rectification at a Metal Semi-conductor Contact. *Phys. Rev.* **1947**, *71*, 717–727.
46. Malagu, C.; Guidi, V.; Stefancich, M.; Carotta, M. C.; Martinelli, G. Model for Schottky Barrier and Surface States in Nanostructured n-Type Semiconductors. *J. Appl. Phys.* **2002**, *91*, 808.
47. Malagu, C.; Guidi, V.; Carotta, M. C.; Martinelli, G. Unpinning of Fermi Level in Nanocrystalline Semiconductors. *Appl. Phys. Lett.* **2004**, *84*, 4158.
48. Ishida, T.; Nagaoka, M.; Akita, T.; Haruta, M. Deposition of Gold Clusters on Porous Coordination Polymers by Solid Grinding and Their Catalytic Activity in Aerobic Oxidation of Alcohols. *Chem.—Eur. J.* **2008**, *14*, 8456–8460.
49. Fukuto, J. M.; Di Stefano, E. W.; Burstyn, J. N.; Valentine, J. S.; Cho, A. K. Mechanism of Oxidation of *N*-Hydroxyphentermine by Superoxide. *Biochemistry* **1985**, *24*, 4161–4167.
50. Yamamoto, T. A.; Nakagawa, T.; Seino, S.; Nitani, H. Bimetallic Nanoparticles of PtM (M = Au, Cu, Ni) Supported on Iron Oxide: Radiolytic Synthesis and CO Oxidation Catalysis. *Appl. Catal., A* **2010**, *387*, 195–202.
51. Liang, D.; Gao, J.; Wang, J.; Chen, P.; Wei, Y.; Hou, Z. Bimetallic Pt–Cu Catalysts for Glycerol Oxidation with Oxygen in a Base-Free Aqueous Solution. *Catal. Commun.* **2011**, *12*, 1059–1062.
52. Uchihara, T.; Matsumura, M.; Yamamoto, A.; Tsubomura, H. Effect of Platinum Loading on the Photocatalytic Activity and Luminescence of Cadmium Sulfide Powder. *J. Phys. Chem.* **1989**, *93*, 5870–5874.
53. Liu, Y.; Tsunoyama, H.; Akita, T.; Xie, S.; Tsukuda, T. Aerobic Oxidation of Cyclohexane Catalyzed by Size-Controlled Au Clusters on Hydroxyapatite: Size Effect in the Sub-2 nm Regime. *ACS Catal.* **2011**, *1*, 2–6.
54. Benfield, R. E. Mean Coordination Numbers and the Nonmetal–metal Transition in Clusters. *J. Chem. Soc., Faraday Trans.* **1992**, *88*, 1107–1110.
55. Arruda, T. M.; Shyam, B.; Ziegelbauer, J. M.; Mukerjee, S.; Ramaker, D. E. Investigation into the Competitive and Site-Specific Nature of Anion Adsorption on Pt Using *In Situ* X-ray Absorption Spectroscopy. *J. Phys. Chem. C* **2008**, *112*, 18087–18097.
56. Wilson, O. M.; Knecht, M. R.; Garcia-Marthinez, J. C.; Crooks, R. M. Effect of Pd Nanoparticle Size on the Catalytic Hydrogenation of Allyl Alcohol. *J. Am. Chem. Soc.* **2006**, *128*, 4510–4511.
57. Murthi, V. S.; Urian, R. C.; Mukerjee, S. Oxygen Reduction Kinetics in Low and Medium Temperature Acid Environment: Correlation of Water Activation and Surface Properties in Supported Pt and Pt Alloy Electrocatalysts. *J. Phys. Chem. B* **2004**, *108*, 11011–11023.
58. Shiraishi, Y.; Tanaka, K.; Shirakawa, E.; Sugano, Y.; Ichikawa, S.; Tanaka, S.; Hirai, T. Light-Triggered Self-Assembly of Gold Nanoparticles Based on Photoisomerization of Spirothiopyran. *Angew. Chem., Int. Ed.* **2013**, *52*, 8304–8308.